Manuscript number: nhess- 2022-253

My co-authors and I would like to express our gratitude to the reviewers for their constructive feedback and suggestions for strengthening our research. The changes we have made to the attached file in response to such feedback and suggestions have been highlighted in blue to facilitate their identification. I would also like to offer my apologies for the length of time it took us to prepare this response. We also record our deep appreciation for the efficient handling of the manuscript.

Response to Reviewer#1

General remarks

I read the manuscript with great interest. Authors have investigated the impact of typhoon Soulik on the coastal ecology, landform, erosion/accretion, suspended sediment movement and associated coastal changes along the Mokpo coast. This research developed an integrated approach for identifying coastal dynamics impacted by typhoons and determining damage severity. Approach and analyses support to derive their conclusions.

The content is interesting for NHESS readers. Overall, the paper is well structured, with results being presented in a clear and organized manner. I have only a few comments and suggestions for improvements.

Thank you for reviewing our manuscript and suggesting that the subject of the manuscript is indeed of interest to NHESS. We considered your suggestions in the revised version of the manuscript, which has undoubtedly improved the contents and structure of the manuscript. Please find detailed responses to your comments.

Comment 1: Sections 3.3 and 3.4 should be discussed under section 3.2, i.e., Typhoon-induced coastal dynamic modeling. Accordingly, subsections should be renumbered and rearranged.

Response: Thank you for your insightful review. In the revised manuscript, sections 3.3 and 3.4 are discussed under section 3.2, and subsections have been renumbered and rearranged accordingly.

Comment 2: Figure 3 and Table 2 contain similar information. It is therefore recommended that Authors keep only one piece of information.

Response: Thank you for your insightful comment. We agreed with the reviewer's suggestion, and Figure 3 has been kept in the revised manuscript.

Comment 3: NDVI and FVC (Fractional vegetation coverage) are frequently used vegetation metrics for assessing land-surface vegetation conditions. Therefore, the use of

NDVI is reasonable for vegetation damage severity mapping. I would expect that Authors should analyze the FVC and compare it to NDVI-derived damaged severity. You are referred to go through the following paper: https://doi.org/10.1007/s11069-018-3351-7.

Response: This is a really interesting point raised by the reviewer. We agreed with the reviewer's suggestion and analyzed FVC in conjunction with NDVI, providing additional insights into vegetation conditions and damage severity. Subsequently, we compared the severity of vegetation damage obtained from both models (i.e., NDVI and FVC). Accordingly, sections 3.2.1 and 4.1.1 have been updated in the revised manuscript as,

3.2.1 Analyses of coastal vegetation loss and disturbance

Vegetation damage severity mapping (VDSM) has been performed using pre-and post-event satellite images. NDVI and FVC are widely used techniques for measuring vegetation density, health status, regional vegetation condition, and detecting vegetation disturbances (Xu et al., 2021; Mishra et al., 2021b; Wang et al., 2010; Yang et al., 2018, Wang and Xu, 2018; Carlson and Ripley, 1997). Subsequently, numerous studies (Xu et al., 2021; Mishra et al., 2021a; Charrua et al., 2021; Shamsuzzoha et al., 2021; Kumar et al., 2021; Nandi et al., 2020; Wang and Xu, 2018; Konda et al., 2018; Zhang et al., 2013; Rodgers et al., 2009) have shown that the NDVI and FVC is a reliable indicator of post-typhoon damage detection. Therefore, in this study, the vegetation damage before and after typhoon Soulik has been determined using the NDVI and FVC approach. The NDVI has been calculated by using the following Eq. (1) (Rouse et al., 1974; Filgueiras et al., 2019):

$$NDVI = \frac{\rho NIR - \rho RED}{\rho NIR + \rho RED} \quad (1)$$

where ρNIR and ρRED are the spectral reflectances corresponding to the eighth (832.8–832.9nm) and fourth (664.6– 664.9nm) Sentinel-2 MSI bands, respectively (Xu et al., 2021). In general, NDVI values range from -1.0 to 1.0; the higher the NDVI value, the better the conditions for vegetation development, and extremely low values indicate the presence of water. Furthermore, the NDVI value above 0.4 indicates vegetated surfaces, and those between 0.25 and 0.40 signify soils with the presence of vegetation (Charrua et al., 2021). The vigor of the vegetation increases as the NDVI values come closer to 1.00 (Rouse et al., 1974). Numerous studies have established the NDVI threshold for vegetated land (e.g., Xu et al., 2021; Wong et al., 2019; Liu et al., 2015; Eastman et al., 2013; Yang et al., 2012; Sobrino et al., 2004). Most researchers noted that the NDVI threshold value for vegetation cover typically ranges from

0.15-2.0 (Xu et al., 2021; Eastman et al., 2013; Sobrino et al., 2004). Therefore, the vegetated pixels (e.g., NDVI threshold > 0.20) present in pre and post-typhoon NDVI images have been used for vegetation severity analysis. The NDVI threshold is considered to reduce the influence of land cover change from the pre-typhoon (2018-08-01) to post-typhoon (2018-10-15) periods.

The degree of vegetation damage has been determined by comparing the NDVI values of the pre-and post-typhoon periods. Various researchers have frequently used the direct difference of NDVI to determine the damage severity caused by typhoons to naturally vegetated land (Wang and Xu, 2018; Konda et al., 2018). It has been calculated on a cell-by-cell basis by subtracting the pre-typhoon NDVI image from that of the post-typhoon in ArcGIS software using map algebra (Zhang et al., 2013; Cakir et al., 2006). The following equation is used to calculate the ΔNDVI (Wang and Xu, 2018),

$$\Delta NDVI = NDVI_{post-typhoon} - NDVI_{pre-typhoon} \quad (2)$$

The difference in NDVI (i.e., ΔNDVI) illustrates the change in natural vegetation, while a negative ΔNDVI value indicates the damage inflicted by a typhoon to the vegetation cover (Xu et al., 2021).

The relative change in NDVI value has been used to investigate the geo-ecological impact on the forest area (Mishra et al., 2021b). The relative vegetation changes ($NDVI_r$) after Soulik have been determined by using the following Eq. (3) (Kumar et al., 2021):

$$NDVI_r = \frac{\Delta NDVI}{NDVI_{pre-typhoon}} \times 100 \quad (3)$$

where the negative $NDVI_r$ value indicates vegetation loss caused by typhoons, and the positive $NDVI_r$ value shows vegetation gain. The $NDVI_r$ value has been classified into three categories corresponding to pixels with decreased, no change, or increased vegetation cover.

On the other hand, we analyze FVC in conjunction with NDVI, which provide additional insights into vegetation conditions and damage severity. Numerous researchers (Wang and Xu, 2018; Song et al., 2017; Bao et al., 2017; Chu et al., 2016; Zhang et al., 2013; Amiri et al., 2009) used FVC to analyze vegetation damage, restoration, recovery, inter-annual variability. It is calculated as the ratio of the area covered by vegetation to the total area of the landscape. It is expressed as a percentage and can range from 0 to 100%. In the present study, FVC was calculated before and after the typhoon using the derived NDVI data (Wang and Xu, 2018). The formula of FVC is as follows (Wang and Xu, 2018; Amiri et al., 2009; Carlson and

Ripley, 1997):

$$FVC = [(NDVI - NDVI_m)/(NDVI_{max} - NDVI_m)]^2 \quad (4)$$

where $NDVI_m$ and $NDVI_{max}$ represent the $NDVI_{min}$ and $NDVI_{max}$ values calculated using equation (1) (Zhang et al., 2021; Ge et al., 2018). The calculated FVC values vary between 0 and 1. After that, the FVC values were converted to percentages to fit the actual FVC classification scheme (Wang and Xu, 2018), which consists of five classes: low (0-20%), medium-low (20-40%), medium (40-60%), medium-high (60-80%), and high (80-100%). Further, the difference in FVC values between the pre-and post-typhoon images was used to calculate the extent of vegetation damage using the following equation:

$$\Delta FVC = FVC_{post-typhoon} - FVC_{pre-typhoon} \quad (5)$$

where ΔFVC is the difference value between the FVC before and after the typhoon. The ΔFVC value represents alterations in vegetation conditions and damage intensity, while a negative value of ΔFVC indicates the extent of damage caused by a typhoon to vegetation cover (Wang and Xu, 2018).

4.1.1 VDSM based on the NDVI and FVC analysis

The VDSM shows the degree of vegetation damage due to typhoons. The comparison of pre-and post-typhoon NDVI and FVC distribution shows a significant loss of vegetated land as the number of no-productivity and low-productivity pixels increases in the post-typhoon NDVI and FVC image.

Figure 5 depicts the spatial distribution of pre and post-typhoon NDVI images. Further, to determine the severity of vegetation damage, the pre-and post-typhoon NDVI image has been classified into six categories, namely non-vegetation (-1.0-0.0), low-vegetation (0.0-0.2), medium-low vegetation (0.2-0.4), medium vegetation (0.4-0.6), medium-high vegetation (0.6-0.8) and high vegetation (0.8-1.0). It was observed that the pre and post-typhoon mean NDVI value was 0.159 and 0.143, respectively, indicating a decline of 0.016 in mean NDVI after the typhoon.

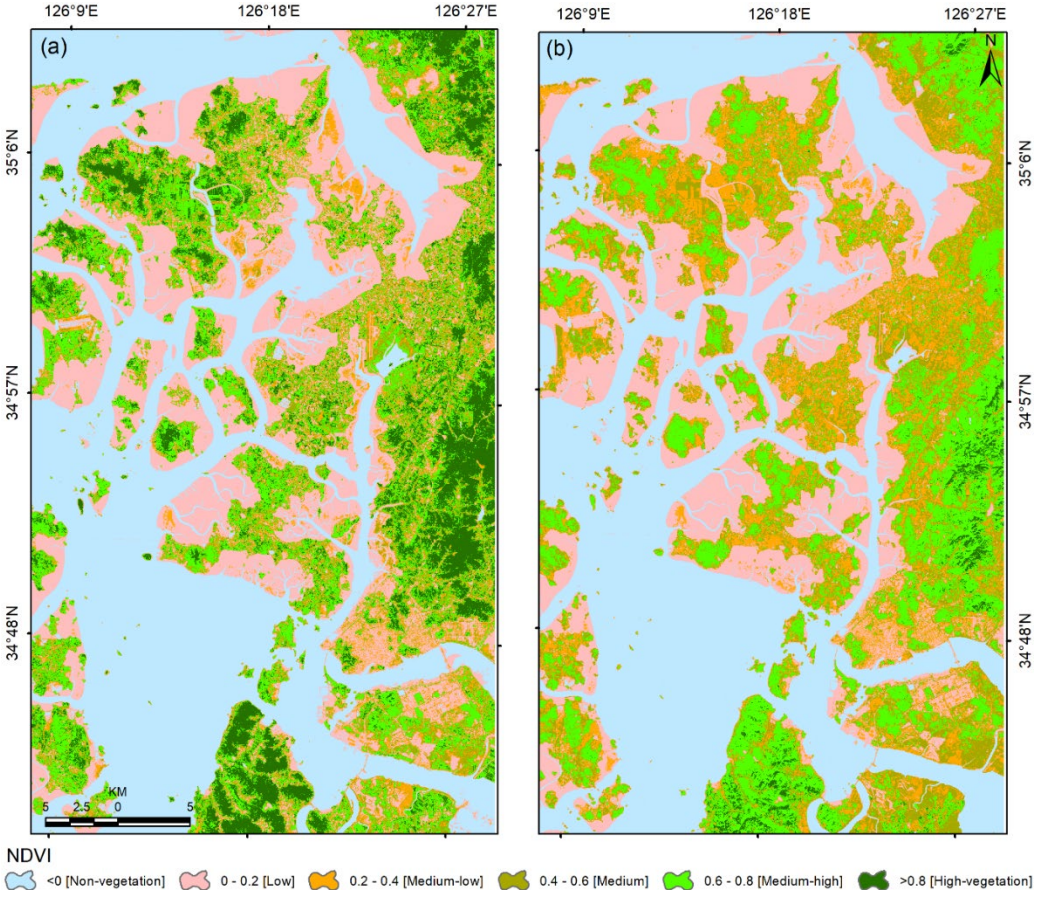

Figure 5. Status of vegetation greenness based on the NDVI data for the (a) pre-Soulik (01st August 2018) and post-Soulik (15th October 2018) period.

Table 3 depicts the area changes for each NDVI category over the typhoon period. It has been observed that the high NDVI values (>0.8) have changed drastically after typhoon-Soulik. The area changes in the low and non-vegetation categories along the Mokpo coastal region revealed that the wetland (mudflat) had accreted after the typhoon. On the other hand, the post-typhoon image was acquired two months after typhoon Soulik, which suggests that the grasses and crops have recovered well. This recovery is reflected in Table 3 from medium-low to medium-high NDVI levels.

Table 3. NDVI distribution over the study area before and after the typhoon.

NDVI levels	Pre-typhoon (km^2)	Post-typhoon (km^2)	Change (km^2)
Non-vegetation (-1 to 0)	673.7	647.6	-26.2
Low (0 to 0.2)	430.4	415.2	-15.2
Medium-low (0.2 to 0.4)	141.6	243.3	101.6
Medium (0.4 to 0.6)	132.5	225.3	92.8

Medium-high (0.6 to 0.8)	283.7	294.4	10.7
High (0.8 to 1.0)	183.6	19.8	-163.8

On the other hand, the physical presence of vegetation has been measured using FVC analysis. In general, NDVI provides information on the health and productivity of vegetation, while FVC provides information on the physical presence and distribution of vegetation. Figure 6 depicts the pre- and post-typhoon FVC map of the Mopko coast. The area of each FVC category is illustrated in Table 4. The results reveal that the typhoon caused a substantial decrease in FVC in the area, with the average FVC reducing significantly from 33.43% to 23.64% after the typhoon. It was observed that the medium-high to high FVC area decreased from 485.4 km^2 to 211.9 km^2, while the medium-to-low FVC area increased from 1359.8 km^2 to 1633.3 km^2. The high FVC vegetation category was more severely affected and decreased considerably after the typhoon. These results indicate that the typhoon significantly impacted the wetland vegetation in the region.

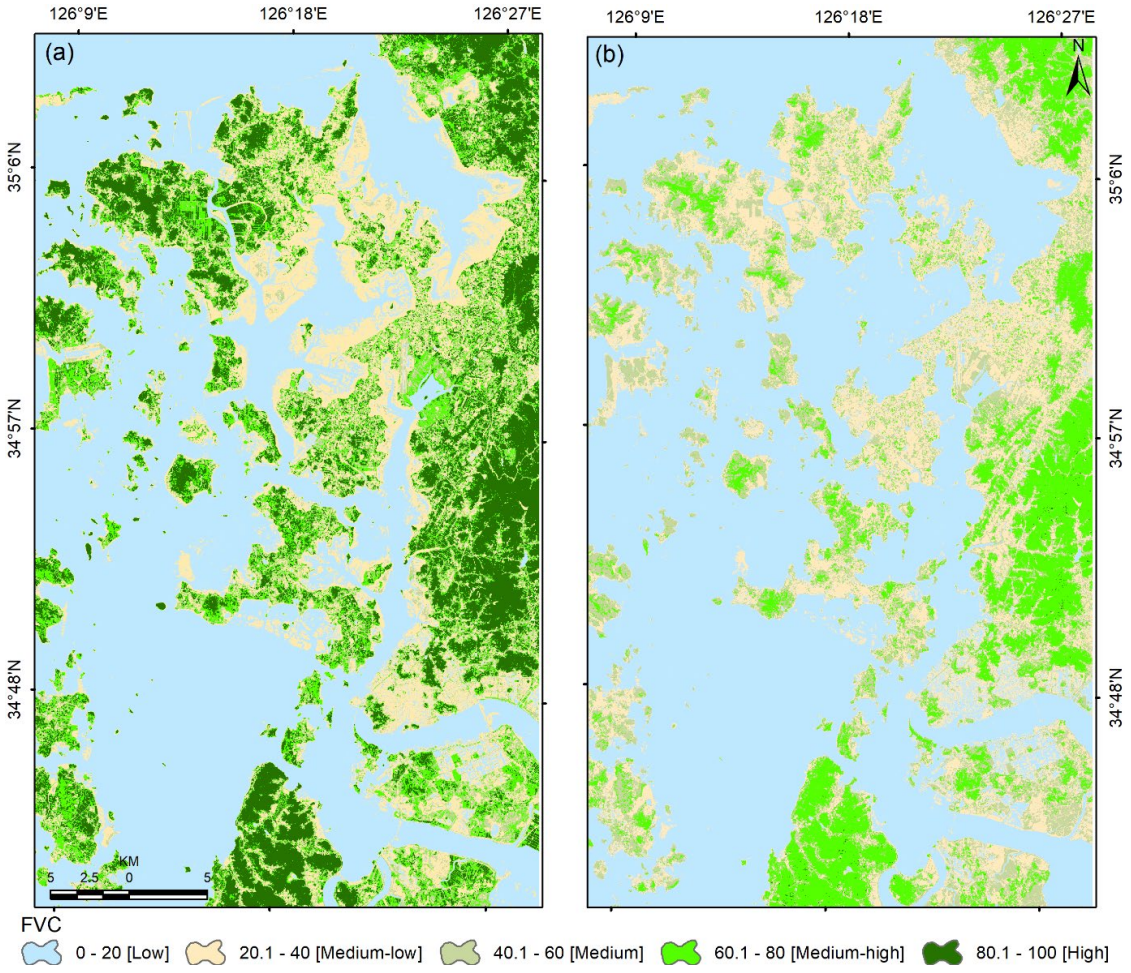

Figure 6. Status of vegetation based on the FVC analysis for the (a) pre-Soulik (01st August 2018) and post-Soulik (15th October 2018) period.

Table 4. Summary of FVC classes before and after the typhoon.

FVC levels (%)	Pre-typhoon (km^2)	Post-typhoon (km^2)	Change (km^2)
Non-vegetation (<20)	890.3	1053.3	162.943
Medium-low (20-40)	327.4	319.6	-7.811
Medium (40-60)	142.4	260.6	118.205
Medium-high (60-80)	206.1	211.5	5.365
High (80-100)	279.4	0.7	-278.671

In order to determine the damaged vegetation areas along the Mokpo coast, we compared pre-and post-typhoon NDVI images. A decrease in ΔNDVI is one of the most distinctive features of abrupt canopy modifications detectable by optical remote sensing (Xu et al., 2021). Thus, we can only determine vegetation deterioration from the two NDVI images. Subsequently, an NDVI threshold of 0.2 has been used to extract only vegetation features from the pre-and post-typhoon NDVI images. The threshold value has been manually adjusted to achieve the highest accuracy of vegetation pixels. The extracted vegetated pixels have been compared with reference samples randomly collected from the original high spatial resolution images to determine the accuracy (Schneider, 2012; Xu et al., 2021). The two extracted vegetation images obtained within six or seven weeks of typhoon Soulik's (i.e., before the damaged vegetation had recovered) exhibits an overall accuracy of 95.7 % for pre-typhoon and 94.5% for the post-typhoon period.

Figure 7(a) depicts the spatial distribution of ΔNDVI, where the highest ΔNDVI indicates a region with highly impacted vegetation areas. The negative ΔNDVI is attributed to about 26.7% of the total area (1845.60 km^2), which suggests that Typhoon Soulik affected approximately 493.98 km^2 of vegetated land. The lowest ΔNDVI value is -0.89, which indicates either tree wind throws or a change in land surface cover from vegetation to build-up land or other non-vegetation covers (Zhang et al., 2013). The results showed that wetland vegetation and agricultural land experienced the most significant NDVI changes, with ΔNDVI values below-0.3. This suggests that these two types of land cover were severely affected by typhoon Soulik.

On the other hand, Figure 7(b) represents the change map derived from the ΔFVC, which also indicates changed vegetation areas after the typhoon. The negative ΔFVC is attributed to about 32.07% of the total area, which suggests that Typhoon Soulik affected approximately 591.89 km^2 of vegetated land. It has also been observed that the pure vegetation

pixels (i.e., NDVI>0.6 and FVC>60%) were drastically changed over the typhoon period. The changed area determined for NDVI and FVC is -153.43 km2 and -273.40 km2, respectively (Tables 3 & 4). The results obtained from both techniques indicate a significant decrease in vegetation cover after the typhoon. The probable reason for the change is that Typhoon Soulik made landfall close to Mokpo coastal region.

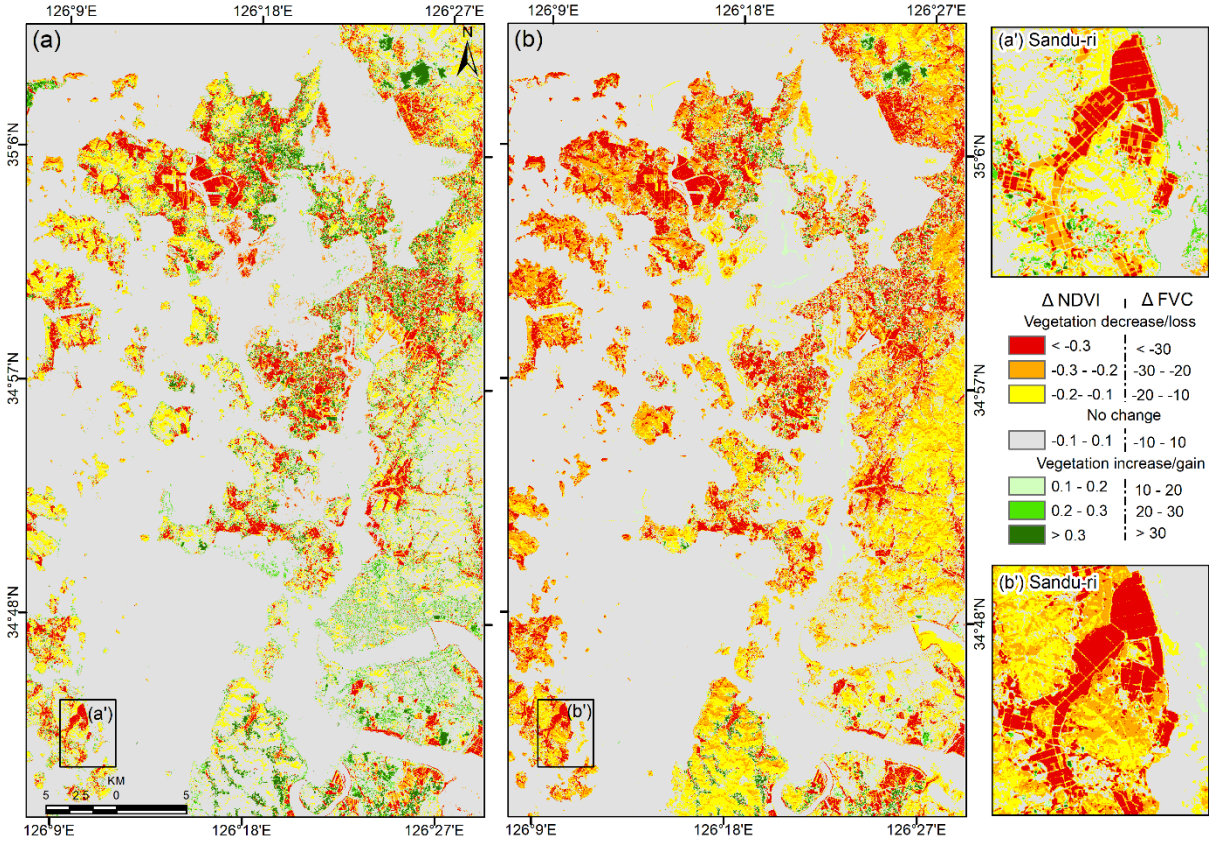

Figure 7. ΔNDVI and ΔFVC derived vegetation change map of the Mokpo coastal region, whereas zoom boxes show the vegetation damage of Sandu-ri areas.

Figure 8 compares vegetation damage based on the number and percentage of the decreased pixel of ΔNDVI and Δ FVC. It exhibits decreased pixels in different categories of vegetation damage, ranging from low damage to extensive damage. The pixels showing the most significant vegetation damage (i.e., ΔNDVI -0.2 to -0.5 and ΔFVC -20 to -50%) account for about 30.9% and 61.5% of the total pixels, respectively. On the other hand, the pixels showing extensive vegetation damage (i.e., ΔNDVI<-0.5 and ΔFVC<-50%) account for only 8.31% and 10.76% of the total pixels. It was observed that the dominant vegetation in the region is wetland vegetation, which is mainly due to the prevalence of wetlands or mudflats in the area. Therefore, the significant vegetation damage implies that wetland vegetation was most severely impacted during typhoons.

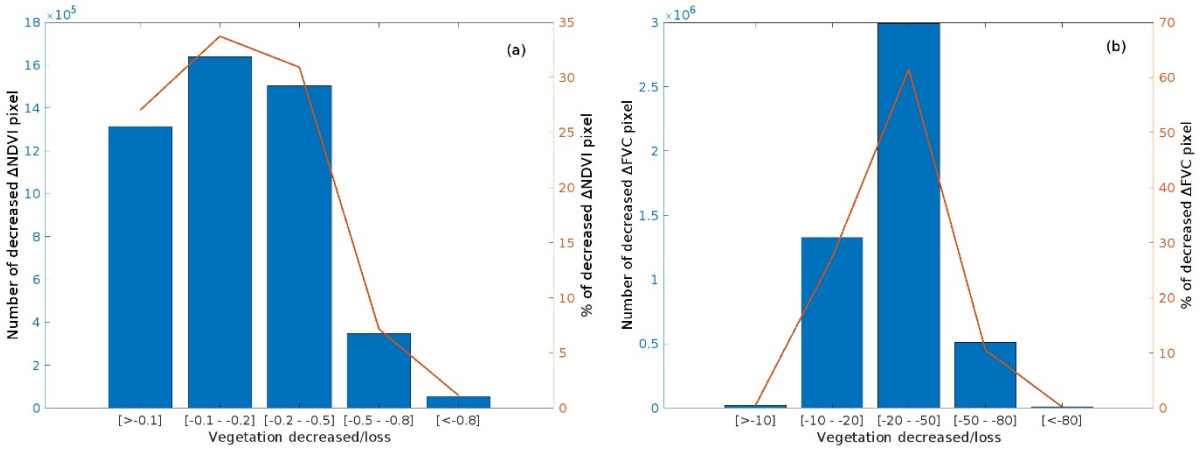

Figure 8. Comparison of vegetation damage represented based on the number and percentage of decreased pixels of (a) ΔNDVI and (b) Δ FVC.

The pre-and post-typhoon Sentinel-2 false-color images and the corresponding relative change in $NDVI_r$ and ΔFVC values are presented in Figure 9. The standard FCC imagery (left panel of Fig. 9) for pre and post-typhoon shows that $NDVI_r$ is more effective in detecting areas of damaged vegetation compared to ΔFVC (right panel, Fig. 9). It was observed that the typhoon-induced damaged vegetation area (i.e., pixels with $NDVI_r$ and ΔFVC of <-50%) detected by $NDVI_r$ (106.5 km^2) was greater than that detected by ΔFVC (51.3 km2). The difference in performance between $NDVI_r$ and ΔFVC in detecting typhoon-induced vegetation damage can be attributed to the fact that the color of the vegetation changed after the typhoon. This change can be detected more accurately by NDVI compared to FVC because the vegetation in the affected areas still existed, and vegetation coverage did not decrease significantly after the event (Wang and Xu, 2018). Thus, NDVI is highly sensitive to the health status of vegetation and a more appropriate approach for assessing the damage to vegetation induced by the typhoon, while FVC is more representative of vegetation coverage status (Wang and Xu, 2018; Jing et al., 2011). Consequently, the dramatic vegetation loss (<-80%) that occurred in mostly wetland vegetation is detected mostly in $NDVI_r$. In addition, moderate greenness loss has been identified in natural forests. Furthermore, the decrease of NDVIr values from higher classes to lower classes indicates that the typhoon has severely damaged the low-lying coastal regions and the wetland vegetation.

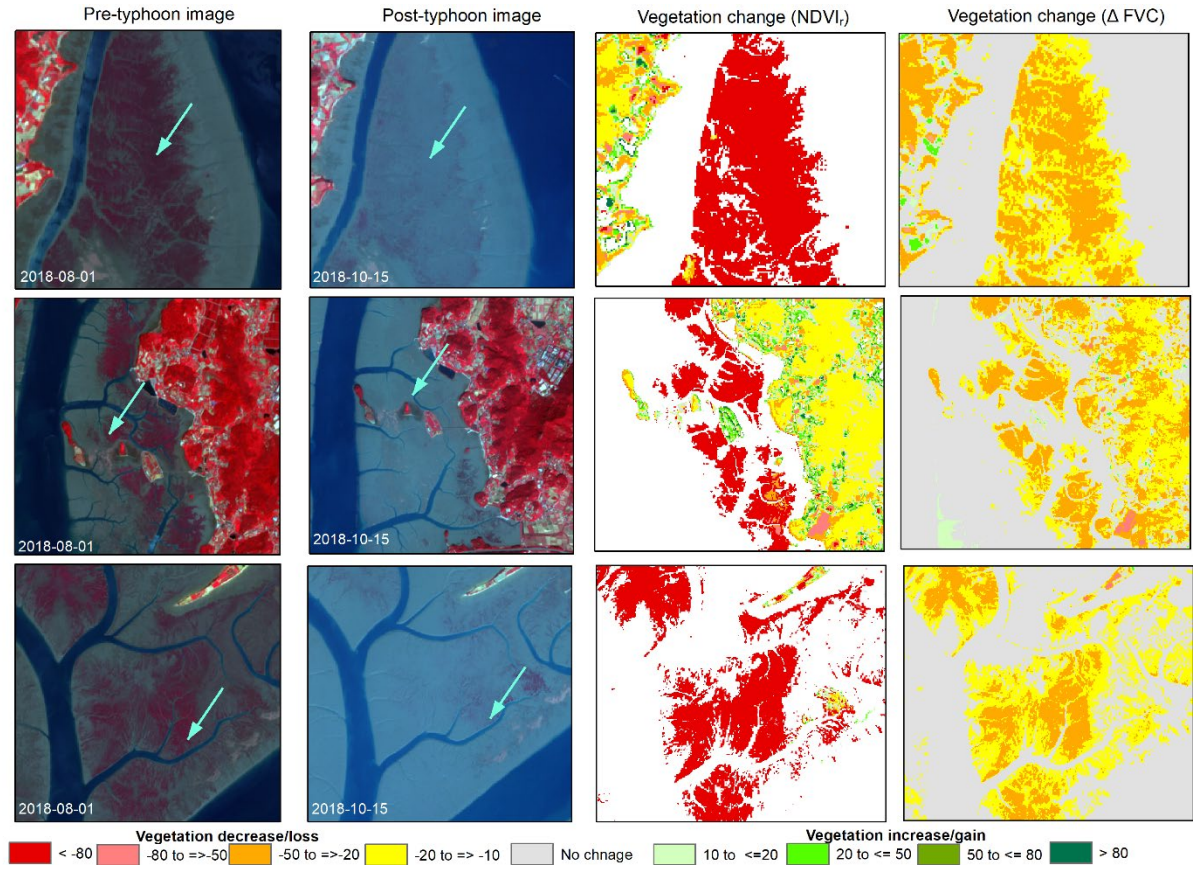

Figure 9. Sentinel-2 MSI standard false color composite images before and after Typhoon Soulik exhibit vegetation damage and the corresponding $NDVI_r$ and ΔFVC (Sentinel-2 MSI level 1C satellite images were downloaded from https://scihub.copernicus.eu/dhus/).

Comment 4: It would be better to explain the influence of topography on vegetation damage caused by Typhoon Soulik.

Response: Thank you for your insightful review. The affected area's topography can influence typhoons' impact on vegetation. The interaction between topography and typhoon-generated wind and rain can result in complex and varied patterns of damage across different landscapes (Abbas et al., 2020; Lu et al., 2020; Zhang et al., 2013). This affect the severity and spatial patterns of vegetation damage. Therefore, the relationship between topography and damaged vegetation has also been established in the present study. For this purpose, high-resolution (5m×5m) DEM data provided by the NGII are used to calculate the region's topographic slope and explore the relationship between topography and typhoon-induced vegetation damage.

It was observed that the elevation varies from 0 to 403 m in the Mopko coastal region, as depicted in Figure 1(b), and the number of trees damaged by Typhoon Soulik showed a decreasing trend at higher elevations (Fig 10a). The highest number of damaged trees was

observed in areas with an elevation of 50m or lower. This is likely due to the fact that these areas are predominantly covered by wetlands, which can be more vulnerable to strong winds associated with typhoons Soulik. In general, low-lying areas may not have the same natural windbreaks and barriers as higher elevations, which can exacerbate the impact of the wind. In addition, low-elevated vegetation may have shallower root systems due to the less stable soil conditions, making them more vulnerable to uprooting during heavy rainfall or strong winds (Zhang et al., 2013; Lugo et al., 1983). A significant difference in the number of decreased ΔNDVI and ΔFVC pixels was observed among different elevation ranges, and a correlation analysis between the number of damaged pixels and elevations showed a negative correlation (i.e., damaged pixels decreased with increasing elevation). The majority of damaged pixels (76.37%) were observed at elevations between 0 and 50m, with a decrease to 13.5% between 51 and 100m. Vegetation decreased rapidly at higher elevations, with the percentage of pixels with negative ΔNDVI and ΔFVC decreasing to 6.1% between 100 and 150m and decreasing to 0.02% between 350 and 403m, as depicted in Figure 10(a).

On the other hand, Figure 10(b) illustrates the extent of damaged vegetation across different slope ranges. It has been noted that there is a negative correlation between the slope and the percentage of damaged vegetation pixels, indicating that the amount of vegetation damage decreases with a higher slope. For instance, when the slope was between 0-5°, approximately 47.63% of vegetation pixels were damaged. As the slope increased, the percentage of damaged vegetation pixels decreased accordingly, with values of 18.15%, 15.01%, 10.71%, 7.74%, 0.73%, and 0.009% observed for slope ranges of 5-10°, 10-15°, 15-20°, 20-30°, 30-40°, and greater than 40°, respectively.

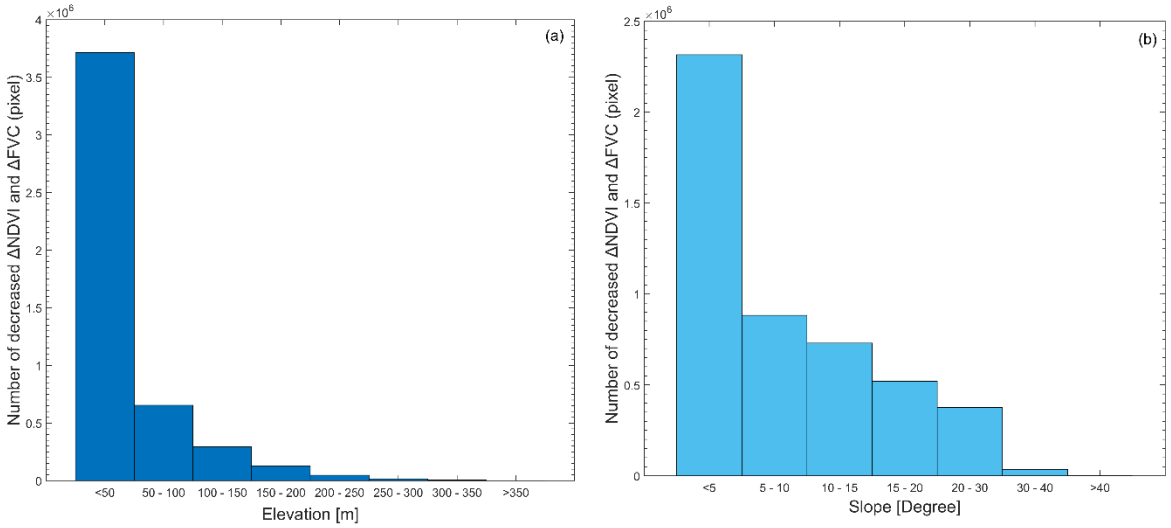

Figure 10. The relationship between topography and vegetation damaged due to typhoon Soulik: (a) numbers of damaged vegetation at different elevation ranges, and (b) numbers of damaged vegetation at different slope ranges.

Comment 5: A statistical summary of the shoreline change based on the NSM model should be presented in a tabular format.

Response: Thank you for your insightful comments. As suggested, the summary of shoreline change statistics based on the NSM model has been incorporated in the revised manuscript.

Table 8: Pre-post typhoon shoreline change statistics based on the NSM model.

NSM statistics	Summary
Total transects	38313
NSM_{mean}	24.24m
$NSM_{mean\ accretion}$	28.89
$NSM_{mean\ erosion}$	-8.29
$NSM_{maximum\ accretion}$	812.54
$NSM_{maximum\ erosion}$	-131.72
Total transect that records accretion	34686
Total transect that records erosion	4955
% of total transect that records accretion	87.5
% of total transect that records erosion	12.5
Overall pre to post-typhoon trend	Accretion

Comment 6: Line 66: The year of the reference in line 66 (Charrua et al., 2020) should be checked.

Response: Thank you for the comment. We have updated the text in the revised manuscript.

Comment 7: Line 112: The year of the reference in line 112 (Kwon et al., 2019) should be checked.

Response: Thank you for the comment. We have updated the text in the revised manuscript.

Comment 8: Line 139: The year of the reference in line 139 (Ryang et al., 2018) should be checked.

Response: Thank you for the comment. We have updated the text in the revised manuscript.

Comment 9: Line 306: The year of the reference in line 306 (Eom et al., 2016) should be checked.

Response: Thank you for the comment. We have updated the text in the revised manuscript.

Comment 10: Lines 335 and 342. Check the abbreviation of remote sensing reflectance.

Response: Thank you for the comment. The remote sensing reflectance (R_r) abbreviation has been checked and updated in the revised manuscript.

Comment 11: Line 461: The unit of measurement in Tables 6 and 7 should be standardized. Choose between sq km or km^2.

Response: Thank you for the comment. The unit of measurement (km^2) in Tables 6 and 7 has been updated in the revised manuscript.

Response to Reviewer#2

General remarks

I found the article interesting, I think it makes important contribution in terms of disaster management caused by coastal erosion. In this study, the results were mapped using various models and index to analyze shoreline and coastal morphodynamics according to typhoons. It has been observed that typhoon-induced suspended sediment concentration influences shoreline and coastal morphology. This paper contributes to understanding natural disasters and their consequences in terms of scientific significance. I have a few comments (general and specific comments) and suggestions for improvements.

We greatly appreciate the critical review of the manuscript and the constructive suggestions put forth by the reviewer that will help improve the quality of the manuscript. We have responded point by point to all the comments and suggestions raised by Reviwer#2 as follows:

Comment 1: Figure 1(a) Is there a reason for showing the population above the basemap? If so, please comment on the difference between the color of the basemap in Figure 1(a) and the color of the basemap in Figure 1(b).

Response: Figure 1(a) is intended to illustrate the population density of the affected area, which is an important factor in understanding the impact of the typhoon on the affected region. On the other hand, the color of the basemap in Figure 1(a) represents the true color image (retrieved from ESRI World Imagery basemap), whereas the color of the basemap in Figure 1(b) represents the post-typhoon standard false-color composite image of the Mokpo coastal region (Sentinel-2 MSI data downloaded from https://scihub.copernicus.eu/dhus/). Both images (Figs. 1(a) and 1(b)) represent the extensive tidal flat region of the Mokpo coast. However, in the revised manuscript, we updated Figure 1 with more scientific exposition, such as province-wise recorded damage and loss distribution (Member Report, 2018), topography variation of the region (NGII, 2018), and variation of significant wave height and wind speed from August 20 to 25, 2018 recorded by Chilbaldo Buoy Station (located near the landfall area) during the typhoon Soulik passage.

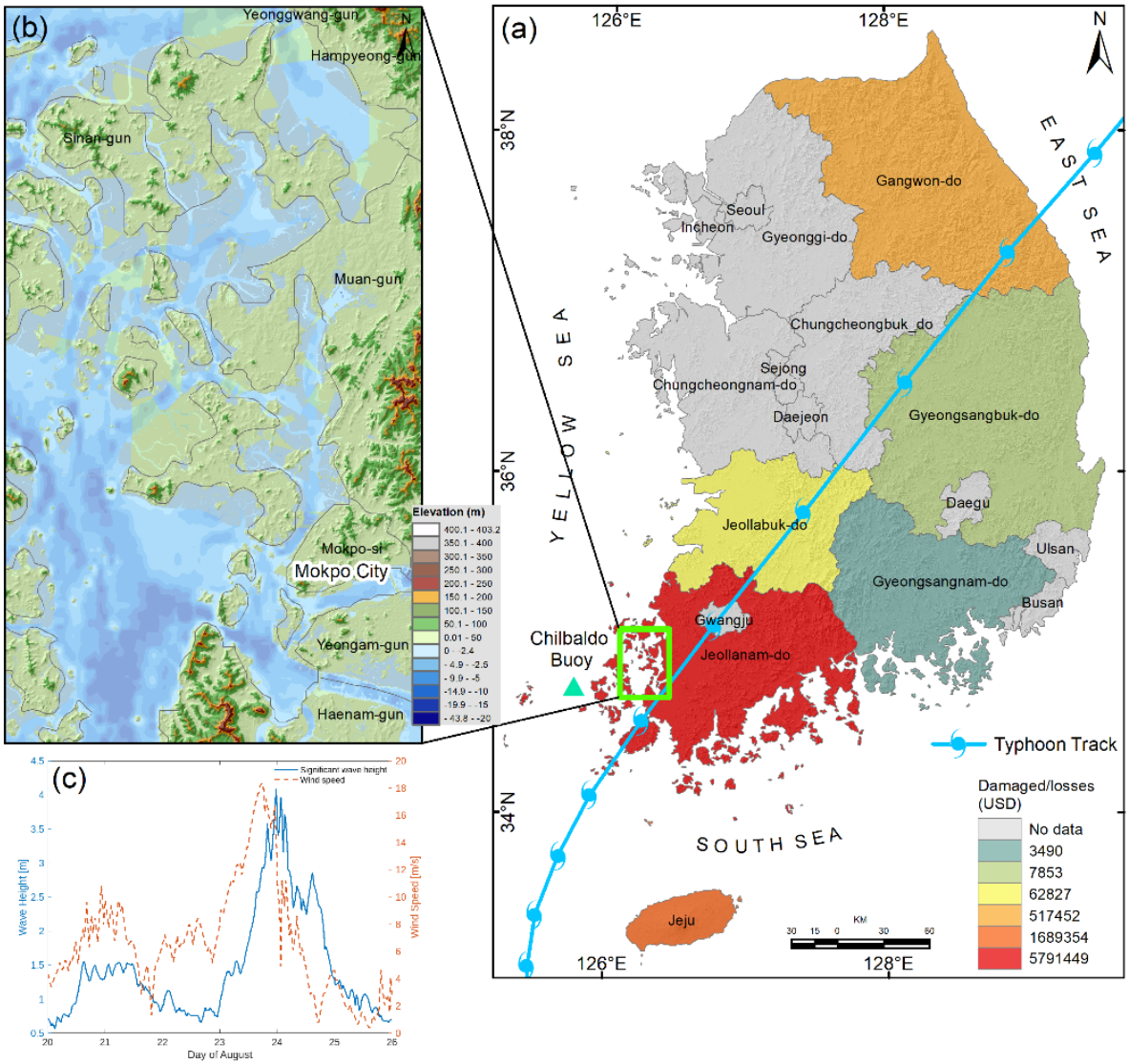

Figure 1. (a) Typhon Soulik passage passed through the Mokpo coastal region on 23rd August 2018 (Typhon track data were downloaded from https://www.ncdc.noaa.gov/ibtracs/), while the background shades represent province-wise recorded damaged/loss distribution reported by Member Report (2018), (b) Topography variation of the Mokpo coastal region (elevation data acquired from NGII (2018), https://www.ngii.go.kr/, and bathymetry data downloaded from GMRT, https://www.gmrt.org), and (c) Variation of significant wave height and wind speed from August 20 to 25, 2018 recorded by Chilbaldo Buoy Station (located near the landfall area) during the typhoon Soulik (Data source: http://wink.kiost.ac.kr/map/map.do#).

Comment 2: It would be better to add images to better understand the data in 3.1 Data Sources.

Response: As suggested, the pre-and post-typhoon standard false color composite images were incorporated in section 3.1 in the revised manuscript as,

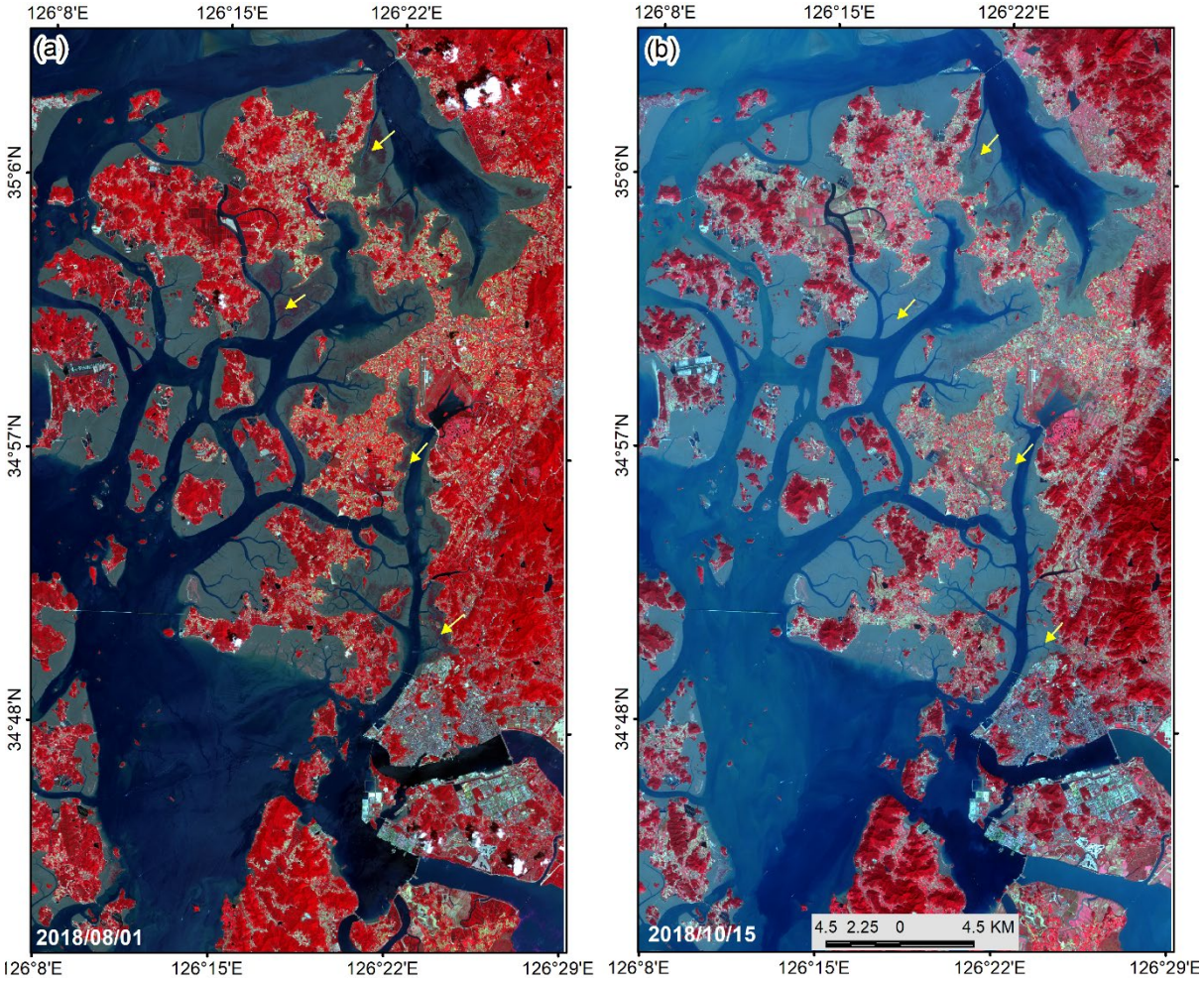

Figure 2. Pre (a) and post-typhoon (b) standard false color composite of reflectance image of the Mokpo coastal region (Sentinel-2 MSI level 1C satellite images are downloaded from https://scihub.copernicus.eu/dhus/). The arrows indicate extensive vegetation damage due to Typhoon Soulik.

Comment 3: Short-term erosion caused by typhoons should be considered for recovery. It is necessary to confirm that the models (net shoreline movement (NSM) and coastal landform change) can predict the recovery of the shoreline and topography after a typhoon. and confidence in the model utilized (comparison with monitoring results, etc.) should also be mentioned.

Response: Thank you for your insightful comment. The recovery status of the Mopko coastal region after typhoon Soulik has been analyzed using the NSM and coastal landform change model. For this purpose, another Sentinel-2 MSI level 1C satellite image was downloaded for October 2019 (one year after the typhoon), as listed in Table 1. After that, the coastal landform change model and NSM were performed based on the Sentinel-2 MSI images of October 2018 and 2019 (both images taken during the post-typhoon period) to understand the recovery status of the coastal morphometry.

The coastal landform change model exhibits that the wetland vegetation increased drastically after one year of typhoon Soulik, as depicted in Figure 16. Table 9 indicates that approximately 16.52% of the land area has accreted over the wetland and water, whereas 39.71% of the wetland vegetation area has accreted over the wetland and water after the typhoon. Further, the outcome of the coastal recovery status was visually compared with the high-resolution aerial imagery downloaded from the National Land Information Platform web portal (https://map.ngii.go.kr/), indicating good consistency. Thus, the coastal landform change model successfully determined the longer-term recovery status in the topography and landforms of the Mopko coastal area after the typhoon.

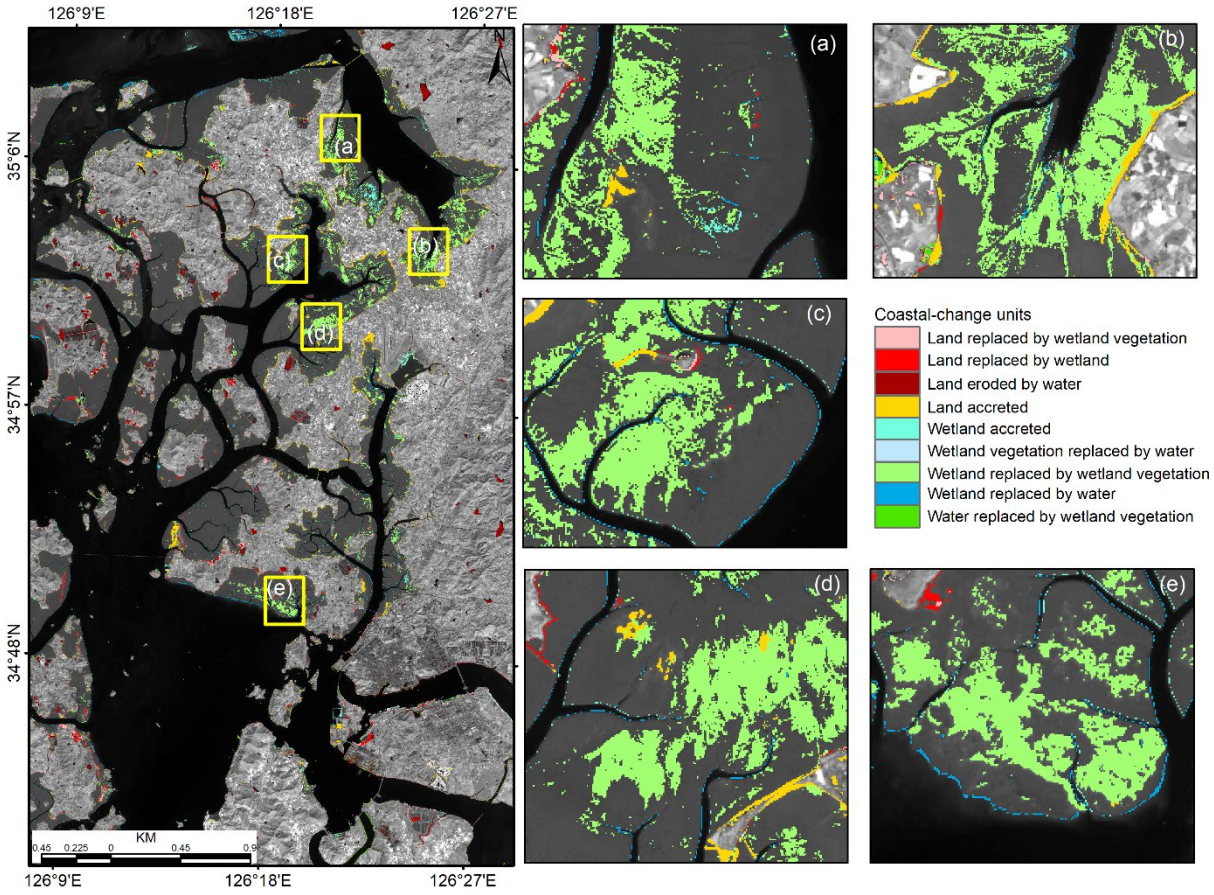

Figure 16. Recovery status of different coastal landforms after typhoon Soulik of Mokpo coastal region, whereas zoom boxes (a-e) show the increase of wetland vegetation at various sites.

Table 9. The details of coastal land transformation classes identify during the post-typhoon the period.

Coastal land transformation	Area (km^2)	%
Land replaced by wetland vegetation	4.06	6.67

Land replaced by wetland	4.59	7.54
Land eroded by water	7.23	11.88
Land accreted	10.05	16.52
Wetland accreted	2.82	4.64
Wetland vegetation replaced by water	2.12	3.48
Wetland replaced by wetland vegetation	24.17	39.71
Wetland replaced by water	4.41	7.25
Water replaced by wetland vegetation	1.41	2.32

On the other hand, the short-term effects of a typhoon on the shoreline have also been determined based on the NSM model. The results exhibit the extensive shoreline alteration in the entire Mokpo coastal region after one year of typhoon Soulik, with an accretion of 48.03% transects and erosion of 51.97%. The NSM statistics showed an average shoreline movement of -1.08m, with a recorded mean erosion of -9.25 and deposition of 7.75m (Table 10). The overall erosion was recorded in response to typhoon Soulik even after one year along the Mopko coastal region. This is due to the extensive damage to wetland vegetation during the typhoon period (Table 7). In addition, it was observed that the wetland experience accretion during the typhoon period, but it made the coastline vulnerable to erosion in the near future. The natural native vegetation and wetland vegetation play a critical role in the shoreline stability of the coastal region due to its anti-erosive nature. This phenomenon was evident in the NSM statistics obtained during the post-typhoon period. Therefore, the use of these models can help predict how the shoreline and adjacent coastal landforms will respond to typhoons, identify vulnerable areas, and inform recovery efforts. This can enhance the area's resilience to natural disasters and reduce the risk of future erosion and other environmental problems.

Table 10. Post-typhoon shoreline change statistics based on the NSM model.

NSM statistics	Summary
Total transects	38313
NSM_{mean}	-1.08m
$NSM_{mean\ accretion}$	7.75
$NSM_{mean\ erosion}$	-9.25
$NSM_{maximum\ accretion}$	44.76
$NSM_{maximum\ erosion}$	-121.14
Total transect that records accretion	18400
Total transect that records erosion	19913
% of total transect that records accretion	51.97
% of total transect that records erosion	48.03
Overall pre to post-typhoon trend	Erosion

Comment 4: The unit of area in Table 7 should be checked.

Response: Thank you for the comment. We have reviewed and updated the unit of area in Table 7 in the revised manuscript.

Comment 5: The table format is not correct. Check it out in its entirety. Text alignment in table should be checked.

Response: Thank you for the comment. We have carefully reviewed the format of all tables in the revised manuscript and made updates wherever necessary.

Comment 6: The position of the legend is not correct for each Figure(Figure 4, 8, 9).

Response: As suggested, the position of the legend of Figures 4, 8, and 9 (now Figs. 5, 12, and 13) has been updated in the revised manuscript as,

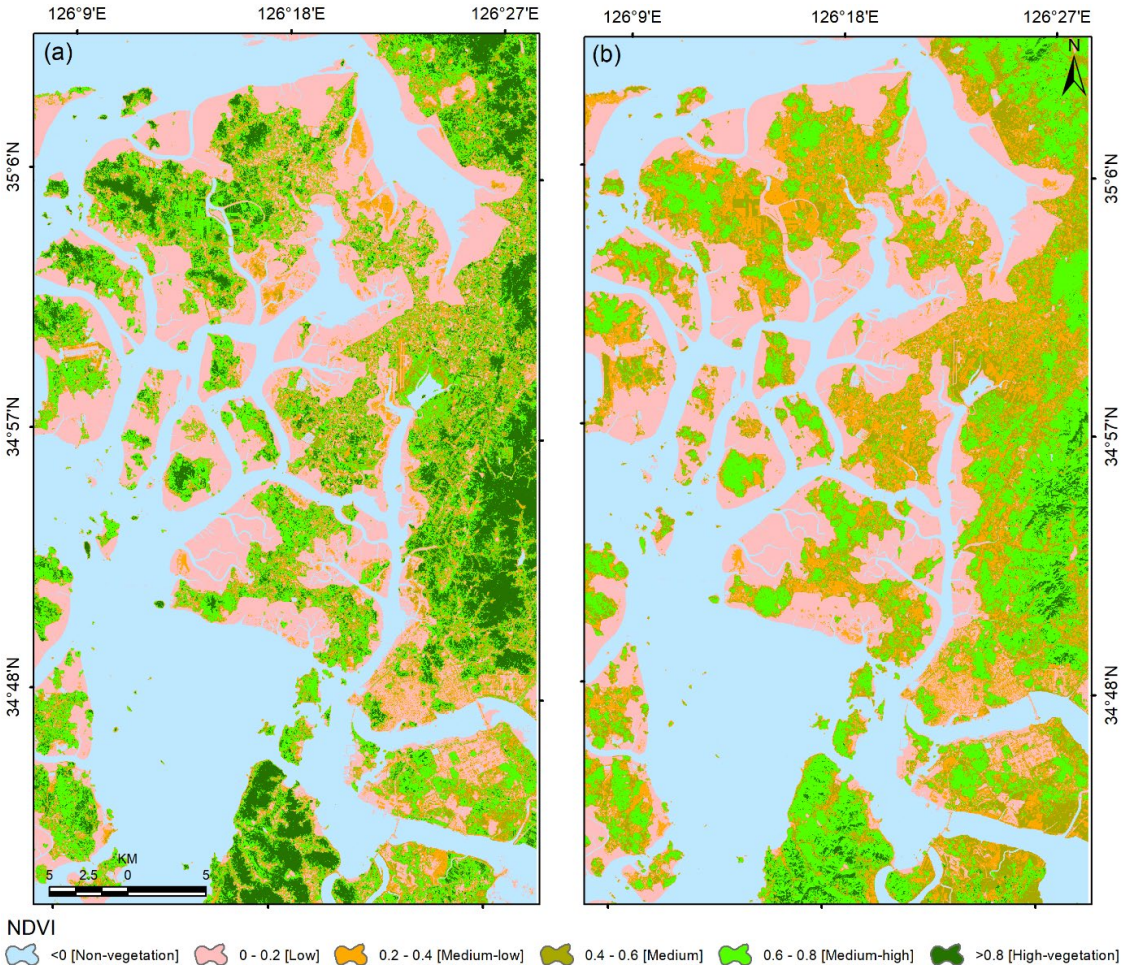

Figure 5. Status of vegetation greenness based on the NDVI data for the (a) pre-Soulik (01st August 2018) and post-Soulik (15th October 2018) period.

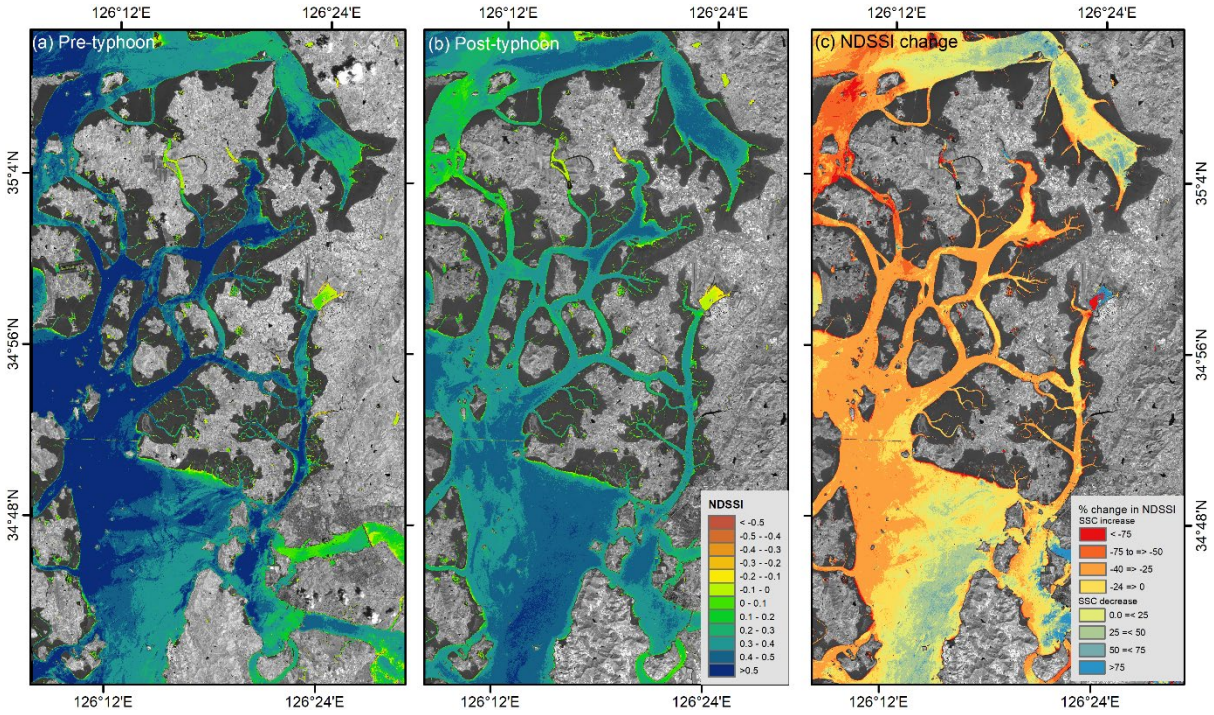

Figure 12. Relative SSC for (a) pre-typhoon and (b) post-typhoon period, while (c) represents the changes in the NDSSI.

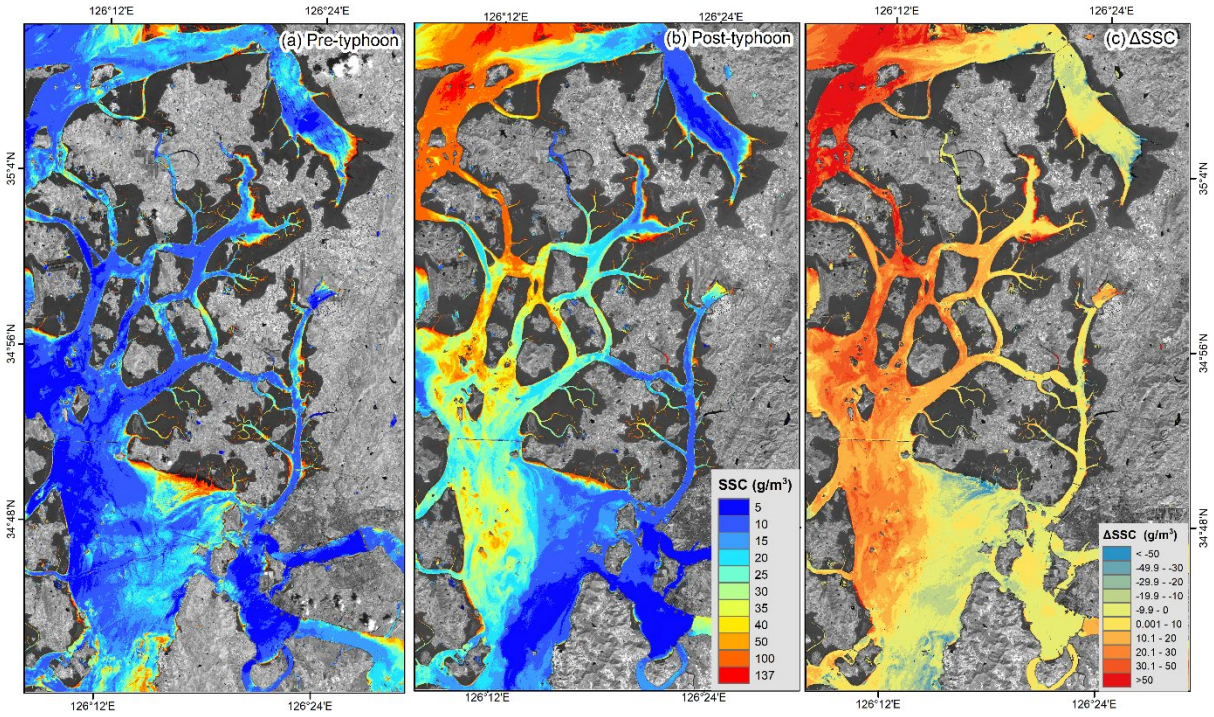

Figure 13. The simulated SSC distribution for the surface water of (a) pre-typhoon, (b) post-typhoon period, and (c) represents the spatial changes of SSC from pre- to post-typhoon.

Comment 7: The detailed title in Figure 11 should be modified for improvement.

Response: Thank you for your comment. The figure caption (Figure 15, revised figure number) has been updated in the revised manuscript as

Figure 15. Net surface area changes (i.e., erosion and accretion) due to typhoon Soulik along the Mokpo coast. Subplots (a-d) show extensive accretion, while erosion is shown in plot (e). The bar graph (f) represents the area changes from the pre to post-typhoon period.

References

Abbas, S., Nichol, J. E., Fischer, G. A., Wong, M. S., and Irteza, S. M.: Impact assessment of a super-typhoon on Hong Kong's secondary vegetation and recommendations for restoration of resilience in the forest succession, Agricultural and Forest Meteorology, 280, 107784, https://doi.org/10.1016/j.agrformet.2019.107784, 2020.

Amiri, R., Weng, Q., Alimohammadi, A., and Alavipanah, S. K.: Spatial–temporal dynamics of land surface temperature in relation to fractional vegetation cover and land use/cover in the Tabriz urban area, Iran, Remote sensing of environment, 113(12), 2606-2617, https://doi.org/10.1016/j.rse.2009.07.021, 2009.

Bao, A., Huang, Y., Ma, Y., Guo, H., and Wang, Y.: Assessing the effect of EWDP on vegetation restoration by remote sensing in the lower reaches of Tarim River, Ecological Indicators, 74, 261-275, https://doi.org/10.1016/j.ecolind.2016.11.007, 2017.

Cakir, H. I., Khorram, S., and Nelson, S. A.: Correspondence analysis for detecting land cover change, Remote Sensing of Environment, 102 (3-4), 306-317, https://doi.org/10.1016/j.rse.2006.02.023, 2006.

Carlson, T. N., and Ripley, D. A.: On the relation between NDVI, fractional vegetation cover, and leaf area index, Remote sensing of Environment, 62(3), 241-252, https://doi.org/10.1016/S0034-4257(97)00104-1, 1997.

Charrua, A. B., Padmanaban, R., Cabral, P., Bandeira, S., and Romeiras, M. M.: Impacts of the tropical cyclone idai in mozambique: A multi-temporal Landsat satellite imagery analysis, Remote Sensing, 13(2), 201, https://doi.org/10.3390/rs13020201, 2021.

Chu, T., Guo, X.,and Takeda, K.: Remote sensing approach to detect post-fire vegetation regrowth in Siberian boreal larch forest, Ecological Indicators, 62, 32-46, https://doi.org/10.1016/j.ecolind.2015.11.026, 2016.

Eastman, J. R., Sangermano, F., Machado, E. A., Rogan, J., and Anyamba, A.: Global trends in seasonality of normalized difference vegetation index (NDVI), 1982–2011, Remote

Sensing, 5(10), 4799-4818, https://doi.org/10.3390/rs5104799, 2013.
Filgueiras, R., Mantovani, E. C., Althoff, D., Fernandes Filho, E. I., and Cunha, F. F. D.: Crop NDVI monitoring based on sentinel 1, Remote Sensing, 11(12), 1441, https://doi.org/10.3390/rs11121441, 2019.
Ge, J., Meng, B., Liang, T., Feng, Q., Gao, J., Yang, S., ... and Xie, H.: Modeling alpine grassland cover based on MODIS data and support vector machine regression in the headwater region of the Huanghe River, China, Remote Sensing of Environment, 218, 162-173, https://doi.org/10.1016/j.rse.2018.09.019, 2018.
Jing, X., Yao, W. Q., Wang, J. H., and Song, X. Y.: A study on the relationship between dynamic change of vegetation coverage and precipitation in Beijing's mountainous areas during the last 20 years, Mathematical and Computer Modelling, 54(3-4), 1079-1085, https://doi.org/10.1016/j.mcm.2010.11.038, 2011.
Konda, V. G. R. K., Chejarla, V. R., Mandla, V. R., Voleti, V., and Chokkavarapu, N.: Vegetation damage assessment due to Hudhud cyclone based on NDVI using Landsat-8 satellite imagery, Arabian Journal of Geosciences, 11(2), 1-11, https://doi.org/10.1007/s12517-017-3371-8, 2018.
Kumar, R., Rani, S., and Maharana, P.: Assessing the impacts of Amphan cyclone over West Bengal, India: a multi-sensor approach, Environmental Monitoring and Assessment, 193(5), 1-21, https://doi.org/10.1007/s10661-021-09071-5, 2021.
Liu, Y., Wu, L., and Yue, H.: Biparabolic NDVI-Ts space and soil moisture remote sensing in an arid and semi-arid area, Canadian Journal of Remote Sensing, 41(3), 159-169, https://doi.org/10.1080/07038992.2015.1065705, 2015.
Lu, L., Wu, C., and Di, L.: Exploring the spatial characteristics of typhoon-induced vegetation damages in the southeast coastal area of China from 2000 to 2018, Remote Sensing, 12(10), 1692, https://doi.org/10.3390/rs12101692, 2020.
Lugo, A. E., Applefield, M., Pool, D. J., and McDonald, R. B.: The impact of Hurricane David on the forests of Dominica, Canadian Journal of Forest Research, 13(2), 201-211, https://doi.org/10.1139/x83-029, 1983.
Member Report: Member Report, Republic of Korea. ESCAP/WMO Typhoon Committee, 13th Integrated Workshop, Chiang Mai, Thailand, 5-9 November 2018 (Avialable at https://www.typhooncommittee.org/13IWS/Members13IWS.html, lat access 28th April, 2023), 2018.
Mishra, M., Acharyya, T., Santos, C. A. G., da Silva, R. M., Kar, D., Kamal, A. H. M., and Raulo, S.: Geo-ecological impact assessment of severe cyclonic storm Amphan on Sundarban mangrove forest using geospatial technology, Estuarine, Coastal and Shelf Science, 260, 107486, https://doi.org/10.1016/j.ecss.2021.107486, 2021a.
Mishra, M., Santos, C. A. G., da Silva, R. M., Rana, N. K., Kar, D., and Parida, N. R.: Monitoring vegetation loss and shoreline change due to tropical cyclone Fani using Landsat imageries in Balukhand-Konark Wildlife Sanctuary, India, Journal of Coastal Conservation, 25(6), 1-11, https://doi.org/10.1007/s11852-021-00840-5, 2021b.
Nandi, G., Neogy, S., Roy, A. K., and Datta, D.: Immediate disturbances induced by tropical cyclone Fani on the coastal forest landscape of eastern India: A geospatial analysis, Remote Sensing Applications: Society and Environment, 20, 100407,

https://doi.org/10.1016/j.rsase.2020.100407, 2020.
NGII: Digital elevation model, NGII (National Geographical Information Institute), the Ministry of Land, Infrastructure and Transport, Korea, 2018.
Rodgers, J. C., Murrah, A. W., and Cooke, W. H.: The impact of Hurricane Katrina on the coastal vegetation of the Weeks Bay Reserve, Alabama from NDVI data, Estuaries and Coasts, 32(3), 496-507, https://doi.org/10.1007/s12237-009-9138-z, 2009.
Rouse, J. W., Haas, J. R. H., Schell, J. A., and Deering, D. W.: Monitoring vegetation systems in the Great Plains with ERTS, In Proceedings of the 3rd ERTS Symposium, Washington, DC, USA, 1, 1974.
Schneider, A.: Monitoring land cover change in urban and peri-urban areas using dense time stacks of Landsat satellite data and a data mining approach, Remote Sensing of Environment, 124, 689-704, https://doi.org/10.1016/j.rse.2012.06.006, 2012.
Shamsuzzoha, M., Noguchi, R., and Ahamed, T.: Damaged area assessment of cultivated agricultural lands affected by cyclone bulbul in coastal region of Bangladesh using Landsat 8 OLI and TIRS datasets, Remote Sensing Applications: Society and Environment, 23, 100523, https://doi.org/10.1016/j.rsase.2021.100523, 2021.
Sobrino, J. A., Jiménez-Muñoz, J. C., and Paolini, L.: Land surface temperature retrieval from LANDSAT TM 5, Remote Sensing of Environment, 90(4), 434-440, https://doi.org/10.1016/j.rse.2004.02.003, 2004.
Song, W., Mu, X., Ruan, G., Gao, Z., Li, L., and Yan, G.: Estimating fractional vegetation cover and the vegetation index of bare soil and highly dense vegetation with a physically based method, International journal of applied earth observation and geoinformation, 58, 168-176, https://doi.org/10.1016/j.jag.2017.01.015, 2017.
Wang, W., Qu, J. J., Hao, X., Liu, Y., and Stanturf, J. A.: Post-hurricane forest damage assessment using satellite remote sensing, Agricultural and forest meteorology, 150(1), 122-132, https://doi.org/10.1016/j.agrformet.2009.09.009, 2010.
Wang, M. and Xu, H.: Remote sensing-based assessment of vegetation damage by a strong typhoon (Meranti) in Xiamen Island, China, Natural Hazards, 93(3), 1231-1249, https://doi.org/10.1007/s11069-018-3351-7, 2018.
Wong, M. M. F., Fung, J. C. H., and Yeung, P. P. S.: High-resolution calculation of the urban vegetation fraction in the Pearl River Delta from the Sentinel-2 NDVI for urban climate model parameterization, Geoscience Letters, 6(1), 1-10, https://doi.org/10.1186/s40562-019-0132-4, 2019.
Xu, S., Zhu, X., Helmer, E. H., Tan, X., Tian, J., and Chen, X.: The damage of urban vegetation from super typhoon is associated with landscape factors: Evidence from Sentinel-2 imagery, International Journal of Applied Earth Observation and Geoinformation, 104, 102536, https://doi.org/10.1016/j.jag.2021.102536, 2021.
Yang, Q., Qin, Z., Li, W., and Xu, B.: Temporal and spatial variations of vegetation cover in Hulun Buir grassland of Inner Mongolia, China, Arid Land Research and Management, 26(4), 328-343, https://doi.org/10.1080/15324982.2012.709215, 2012.
Yang, Y., Erskine, P. D., Lechner, A. M., Mulligan, D., Zhang, S., and Wang, Z.: Detecting the dynamics of vegetation disturbance and recovery in surface mining area via Landsat imagery and LandTrendr algorithm, Journal of Cleaner Production, 178, 353-362,

https://doi.org/10.1016/j.jclepro.2018.01.050, 2018.
Zhang, X., Wang, Y., Jiang, H., and Wang, X.: Remote-sensing assessment of forest damage by Typhoon Saomai and its related factors at landscape scale, International Journal of Remote Sensing, 34(21), 7874-7886, https://doi.org/10.1080/01431161.2013.827344, 2013.
Zhang, J., Zhang, Z., Chen, J., Chen, H., Jin, J., Han, J., ... and Wei, G.: Estimating soil salinity with different fractional vegetation cover using remote sensing, Land Degradation & Development, 32(2), 597-612, https://doi.org/10.1002/ldr.3737, 2021.